Leap-frog patterns in systems of two coupled FitzHugh-Nagumo units

Sebastian Eydam,[1,*] Igor Franović,[2] and Matthias Wolfrum[1]
[1]*Weierstrass Institute for Applied Analysis and Stochastic, Mohrenstrasse 39, 10117 Berlin, Germany*
[2]*Scientific Computing Laboratory, Center for the Study of Complex Systems, Institute of Physics Belgrade, University of Belgrade, Pregrevica 118, 11080 Belgrade, Serbia*

(Received 17 January 2019; published 12 April 2019)

We study a system of two identical FitzHugh-Nagumo units with a mutual linear coupling in the fast variables. While an attractive coupling always leads to synchronous behavior, a repulsive coupling can give rise to dynamical regimes with alternating spiking order, called leap-frogging. We analyze various types of periodic and chaotic leap-frogging regimes, using numerical path-following methods to investigate their emergence and stability, as well as to obtain the complex bifurcation scenario which organizes their appearance in parameter space. In particular, we show that the stability region of the simplest periodic leap-frog pattern has the shape of a locking cone pointing to the canard transition of the uncoupled system. We also discuss the role of the timescale separation in the coupled FitzHugh-Nagumo system and the relation of the leap-frog solutions to the theory of mixed-mode oscillations in multiple timescale systems.

DOI: 10.1103/PhysRevE.99.042207

I. INTRODUCTION

The FitzHugh-Nagumo system is a classical model of neuronal dynamics. As the simplest, yet paradigmatic example of a coupled neuronal system, we investigate here a pair of two identical FitzHugh-Nagumo units with a weak mutual coupling. Such a network motif of two coupled neurons has been considered as a basic building block of central pattern generators [1] and the complex neural networks of the cortex [2–5]. The dynamics of such systems has typically been investigated in the framework of the synchronization paradigm [6–8], focusing on the stability of states with phase-locked firing and their potential role in rhythmogenesis [9]. Nevertheless, a remarkable property of these simple circuits is that they are also able to generate complex activity patterns where the interspike intervals show complex dynamics. A typical example of such patterns is the so-called leap-frog dynamics [10], sometimes also called leader-switching dynamics [11], where the units exchange their order of firing within each oscillation cycle. Such a regime has so far been associated exclusively to class I neural oscillators coupled via strong synapses with complex nonlinear dynamics [12–16]. In the present paper, we investigate the emergence of leap-frogging dynamics in a system of two classical FitzHugh-Nagumo units interacting only via a small linear coupling. The emerging complex dynamical patterns can be explained as a result of the timescale separation between the activator and the recovery variable. For a single unit, the timescale separation is crucial for the mechanism inducing the rapid change in the amplitude from small subthreshold oscillations to large relaxation oscillations. Introducing a repulsive coupling in the fast variables, the leap-frog patterns emerge in locking cones generated by a complex bifurcation scenario immediately at this transition. The alternation in the spiking order of the units arises from trajectories containing both the small-amplitude subthreshold oscillations and the large-amplitude relaxation oscillations. Such a behavior involving interspersed small- and large-amplitude oscillations, called *mixed-mode oscillations* [17–20], is a typical phenomenon in slow-fast systems with at least two slow variables and has been studied extensively by geometric singular perturbation methods for the limit of infinite timescale separation. In particular, a three-dimensional version of the FitzHugh-Nagumo system has been used as a classical example for mixed-mode oscillations, see, e.g., Ref. [20] and references therein. Singular perturbation techniques have been also applied to coupled nonidentical mixed-mode oscillators [21] and for the synchronization of weakly coupled slow-fast oscillations [22].

Coupled systems of two identical oscillators have specific symmetry properties, which at vanishing coupling induce an additional degeneracy. First numerical studies of coupled slow-fast oscillators can already be found in Refs. [23,24], where a detailed exposition of the four-dimensional slow-fast structure is given. Due to the symmetry-induced degeneracy, for such systems the existing theoretical results for mixed-mode oscillations do not apply directly. We will present here a first numerical exploration of a system of two identical FitzHugh-Nagumo units with symmetric mutual coupling. Our approach will be a detailed bifurcation analysis using path-following methods at finite values of the timescale separation. We perform this both for the degenerate case of small coupling, where we find an essentially new dynamical scenario, and for larger coupling, where the leap-frog dynamics is organized in a way that conforms to the general results on mixed-mode oscillations.

*sebastian.eydam@wias-berlin.de

The dynamics of the considered system of two identical FitzHugh-Nagumo units is given by

$$\begin{aligned}\frac{dv_{1,2}}{dt} &= v_{1,2} - v_{1,2}^3/3 - w_{1,2} + c(v_{2,1} - v_{1,2}),\\ \frac{dw_{1,2}}{dt} &= \varepsilon(v_{1,2} + b),\end{aligned} \tag{1}$$

where the symmetric linear coupling acts in the fast variables $v_{1,2}$. The small parameter ε facilitates the timescale separation between the fast variables v_i and the slow variables w_i. In the context of neuroscience, the former represent the neuronal membrane potentials, whereas the latter correspond to the coarse-grained activities of the membrane ion-gating channels. For a single unit, the parameter b mediates the transition from the quiescent regime for $b > 1$ to the oscillatory regime for $-1 < b < 1$. Due to the timescale separation, this is accompanied by a *canard transition* from small-amplitude subthreshold oscillations to the large-amplitude relaxation oscillations. We invoke some basic results derived from singular perturbation theory about the slow-fast structure of the uncoupled FitzHugh-Nagumo unit in Sec. II.

Since the parameters b and ϵ are taken to be identical for both units, system Eq. (1) possesses a $\mathbb{Z}_2$-symmetry, being equivariant with respect to exchanging the indices by

$$\sigma : (v_1, w_1, v_2, w_2) \mapsto (v_2, w_2, v_1, w_1).$$

This leads to the appearance of solutions with different symmetry types, reflecting the different states of in-phase and anti-phase synchronization, which will be discussed in Sec. II which concerns the basic types of solutions bifurcating from the stationary regime. Close to the canard transition of the uncoupled system, there appear various types of periodic and chaotic leap-frog patterns in the system with repulsive coupling. Using the software package AUTO [25] for numerical bifurcation analysis by continuation methods, in Sec. III we investigate in detail the complex bifurcation scenarios responsible for the onset of the different types of leap-frogging dynamics. We conclude the paper with an outlook in Sec. IV, discussing the relation of our results to earlier findings on leap-frog dynamics in models of neuronal systems.

II. BASIC DYNAMICAL REGIMES

We begin our investigation of system Eq. (1) by collecting simple stationary and periodic solutions together with their stability and symmetry properties. In the symmetric regime

$$v_1 = v_2 \quad \text{and} \quad w_1 = w_2, \tag{2}$$

the coupling term vanishes and the dynamics Eq. (1) is governed by a single FitzHugh-Nagumo system, where the units display simultaneously the well-known transition from the quiescent regime with a unique stable equilibrium for $b > 1$ to the oscillatory regime for $b < 1$, mediated by a supercritical Hopf bifurcation at $b = 1$. Due to the timescale separation $0 < \varepsilon \ll 1$, the bifurcating branch of periodic solutions displays a characteristic transition from small-amplitude harmonic oscillations of period $O(1/\sqrt{\varepsilon})$ to large-amplitude relaxation oscillations of period $O(1/\varepsilon)$, called a *canard transition*. This scenario has been extensively studied within the framework of singular perturbation theory, viz. in the limit $\varepsilon \to 0$; see, e.g., Ref. [18] for a recent overview. In Fig. 1 we illustrate the canard transition in the symmetric regime, showing numerical results obtained by path-following methods [25]. In Fig. 1(a) we have fixed $\varepsilon = 0.05$, displaying the varying period along the branch of periodic orbits emerging from the Hopf-bifurcation at $b = b_H = 1$. Note the nearly vertical transition from small to large periods at the canard transition $b = b_c$. The phase portraits of the three orbits shown in Fig. 1(b), selected before, after, and immediately at the transition, indicate that the change in the period is accompanied by a transition from small to large amplitudes via *canard trajectories* that follow the unstable part of the slow manifold, which is close to the critical manifold $w = v - v^3/3$. From the neuroscience perspective, this corresponds to a transition route from the quiescent state to the spiking regime via subthreshold oscillations. A detailed asymptotic analysis reveals that the leading order approximation for the location b_c of the canard transition is given by

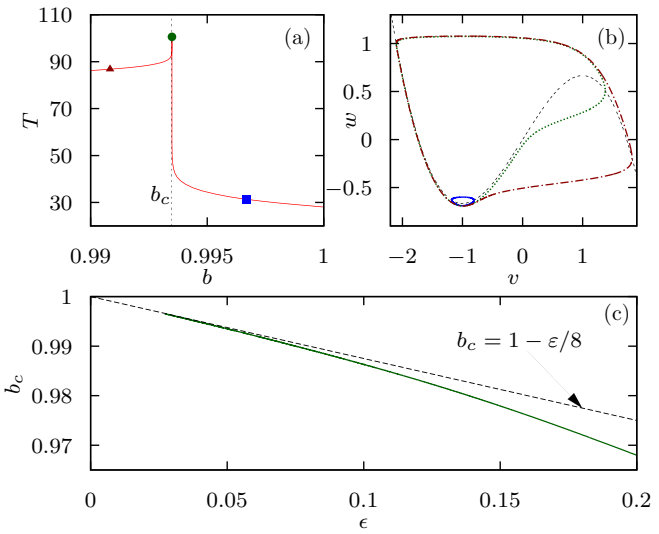

FIG. 1. (a) Variation of the period T along the branch of synchronous periodic solutions for varying b and fixed $\varepsilon = 0.05$. (b) Phase portraits of selected periodic solutions: a subthreshold oscillation for $b_c < b < b_H$ (blue solid), the canard trajectory $b_c = b$ (green dotted), a relaxation oscillations with $b_c > b$ (red dotted-dashed), corresponding to the square, the triangle, and the disk, in (a) respectively, and the cubic nullcline (dashed black). The corresponding values of b are indicated by the colored dots in (a). (c) Location of the canard transition b_c for varying ε. Numerical path-following of the periodic solution with maximal period (green line) is compared to asymptotic formula Eq. (3), shown dashed.

$$b_c \approx (1 - \varepsilon/8), \tag{3}$$

see Ref. [26]. In Fig. 1(c) we show that for small $\varepsilon > 0$ this expression (dashed line) provides indeed a good approximation for the actual location of the canard transition (solid green line), which we obtained numerically by path-following in ε the trajectory of maximal period, sometimes called *maximal canard* [green curve in Fig. 1(b)]. Recall that both the regimes of stable equilibrium and of subthreshold oscillations are excitable [27,28] in a sense that a strong enough perturbation

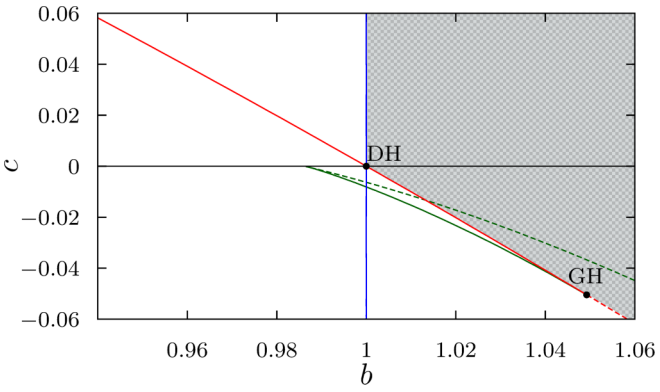

FIG. 2. Stability region (checkered pattern) of the symmetric equilibrium Eq. (5) in the (b, c) plane, bounded by in-phase Hopf instability (vertical blue line) and antiphase Hopf instability (diagonal red line). The antiphase Hopf bifurcation changes from supercritical to subcritical in a generalized Hopf point (GH), where a fold curve of the antiphase synchronous limit cycles emerges (green line). DH denotes the resonant double Hopf point for the decoupled system at $(b, c) = (1, 0)$.

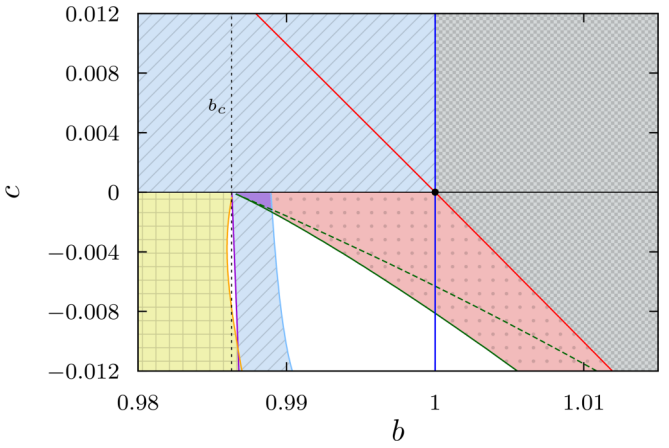

FIG. 3. Stability regions of basic periodic solutions in the (b, c) plane for $\varepsilon = 0.1$: in-phase synchronous oscillations (blue diagonal stripes); antiphase synchronous subthreshold oscillations (red dotted); coexistence of in-phase and antiphase subthreshold oscillations (purple filled); asynchronous oscillations—successive spiking (yellow squared). Bifurcation curves delineating the stability boundaries: in-phase Hopf instability (vertical blue line); antiphase Hopf instability (diagonal red line); fold of antiphase synchronous limit cycles (left boundary of the lower dotted region, green); subcritical period doubling of in-phase subthreshold oscillations (left boundary of the lower striped region, purple); subcritical symmetry breaking pitchfork of in-phase subthreshold oscillations (right boundary of the lower striped region, light blue); supercritical period doubling of asynchronous oscillations (boundary of the squared region, orange). Canard transition at $b = b_c$ (black dashed); see Fig. 1.

may elicit a large excursion in phase space, i.e., a spiking response in the form of a single relaxation oscillation.

The full system Eq. (1), which can be rewritten in coordinates longitudinal and transversal to the symmetry subspace Eq. (2),

$$v_{L,T} = v_1 \pm v_2, \quad w_{L,T} = w_1 \pm w_2, \tag{4}$$

has a slow-fast structure with two fast and two slow variables. For small coupling c, the corresponding critical manifolds and fast fibers are given trivially as a direct sum of the corresponding objects for each of the units. It can be easily seen that the only stationary state of Eq. (1) is the symmetric equilibrium

$$(v_1, w_1, v_2, w_2) = (-b, -b + b^3/3, -b, -b + b^3/3), \tag{5}$$

obtained from the single FitzHugh-Nagumo unit. While the symmetry-preserving Hopf bifurcation at $b = 1$ in the coupled system is analogous to the Hopf bifurcation of the single FitzHugh-Nagumo unit and does not depend on the coupling parameter c, in the coupled system the symmetric equilibrium may also undergo symmetry-breaking bifurcations. In particular, it may become unstable via a Hopf bifurcation to antiphase synchronized periodic solutions of the form

$$v_1(t) = v_2\left(t + \frac{T}{2}\right), \quad w_1(t) = w_2\left(t + \frac{T}{2}\right), \tag{6}$$

where $T > 0$ is the period. Using the longitudinal and transversal coordinates Eq. (4) one obtains the condition

$$c = \frac{1 - b^2}{2} \tag{7}$$

for this antiphase Hopf instability of the synchronous equilibrium Eq. (5). In Fig. 2, the associated bifurcation curve is shown in the (b, c) plane together with the in-phase Hopf instability at $b = 1$. For attractive coupling $c > 0$, the stability region (checkered pattern) of the symmetric equilibrium Eq. (5) is bounded by the in-phase Hopf instability, shown by the blue line, while for repulsive coupling $c < 0$, the stability boundary is given by the antiphase Hopf Eq. (7). For larger negative values of c, this bifurcation is subcritical, such that no stable branch of antiphase synchronized oscillations emerges. The criticality changes in a generalized Hopf (Bautin) point, labeled as GH in Fig. 2. From this point emanates a curve of folds of limit cycles, shown by the green line in Fig. 2. The two Hopf bifurcation curves intersect in the resonant double Hopf point (DH) located at $(b, c) = (1, 0)$. Note that this point belongs to the line $c = 0$ where the system decouples, thus behaving neutral with respect to all symmetry-breaking perturbations.

Figure 3 shows the stability regions and the associated stability boundaries of the periodic solutions. For attractive coupling $c > 0$, all synchronous oscillations are stable (blue diagonal striped region), undergoing at $b = b_c$ the canard transition from small- to large-amplitude oscillations as in the case of a single unit; cf. Fig. 1. For repulsive coupling $c < 0$, the situation is more complicated. There is a small region (red dotted in Fig. 3) above the generalized Hopf point and the emanating fold of limit cycles (green curve) where one finds stable antiphase synchronized oscillations. Note that after a secondary bifurcation, the fold of limit cycles (green curve) is no longer a stability boundary of the antiphase synchronized oscillations (dashed part of the curve). Surprisingly, there are also stable in-phase synchronized solutions for repulsive coupling $c < 0$. They are confined to a narrow region immediately below the canard transition, which is bounded by a curve of period doubling (left, purple line) and

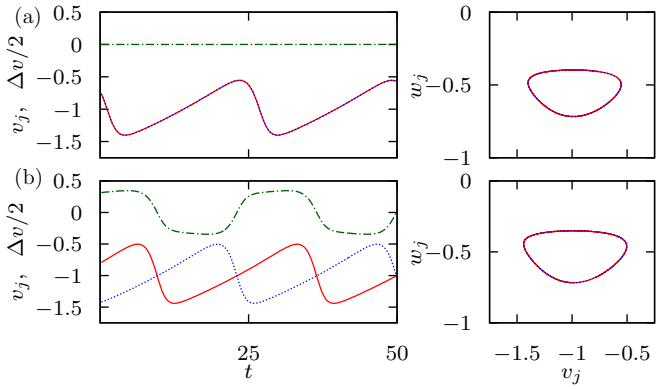

FIG. 4. Time traces and phase portraits of stable coexisting in-phase synchronous (a) and antiphase synchronous (b) subthreshold oscillations. Parameters $(\varepsilon, b, c) = (0.1, 0.9885, -0.0005)$ belong to the coexistence region (purple in Fig. 3). Variables $v_{1,2}(t)$ are shown in red (solid) and blue (dotted), whereas the coupling term $\Delta v = c(v_2 - v_1)$ is indicated in green color (dash-dotted).

a curve of symmetry-breaking pitchfork bifurcations (right, light blue line). In particular, for small negative coupling, one encounters a region of bistability, where both the in-phase and antiphase synchronized oscillations are stable (purple-shaded region in Fig. 3). Figure 4 illustrates coexisting stable in-phase and antiphase synchronous solutions computed for the parameters $(\varepsilon, b, c) = (0.1, 0.9885, -0.0005)$ from this region. Note that the coexistence region is confined to subthreshold oscillations prior to the canard transition at $b = b_c$.

Apart from the in-phase and antiphase synchronous regimes, there may also appear periodic solutions without any symmetry. For repulsive coupling $c < 0$ and beyond the canard transition, i.e., $b < b_c$, there is a large parameter region admitting a stable regime of *successive spiking*, with both units performing relaxation oscillations shifted in phase. The stability region of this successive spiking, shown in yellow (square pattern) in Fig. 3, is bounded by a curve of supercritical period doubling (right, orange line). Figures 5(a) and 5(b) provide the time traces and phase portraits for the regime of

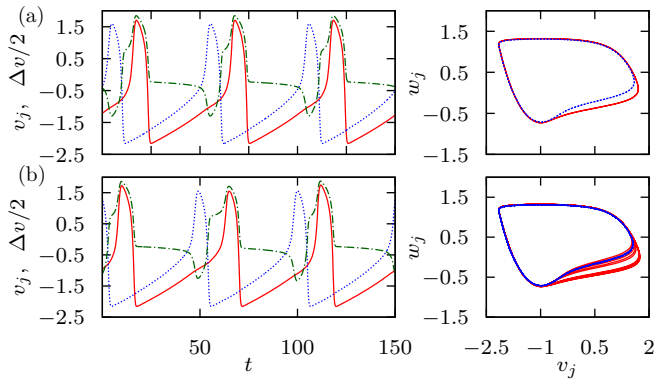

FIG. 5. Time traces and phase portraits of stable asymmetric successive spiking: (a) before period doubling ($b = 0.98625$) and (b) after several period doubling bifurcations ($b = 0.98692$). The remaining parameters are $(c, \varepsilon) = (-0.01, 0.1)$. Colors and line styles are as described in the caption of Fig. 4.

successive spiking before period doubling and after several period doubling bifurcations, respectively. Note that in Fig. 3 several bifurcation curves point toward the canard transition, thus creating a complex scenario where the different dynamical regimes with different symmetry properties bifurcate and interchange their stability. This indicates that a detailed study of the limit $\varepsilon \to 0$, $c \to 0$ could reveal the dependence of all these bifurcations on ε and in this way explain the whole scenario by an unfolding of the corresponding singularity.

Moreover, there is a region, indicated in white in Fig. 3, where none of the periodic solutions described above is stable. We demonstrate below that in this region the system exhibits several periodic or chaotic regimes characterized by the fact that the trajectory of each unit comprises large relaxation oscillation loops as well as smaller loops of a size comparable to that of subthreshold oscillations. This phenomenon of such so called mixed-mode oscillations has been extensively studied using geometric singular perturbation methods for the limit $\varepsilon \to 0$. They are known to arise generically in slow-fast systems with two slow variables and a folded node singularity. Let us very briefly recall the corresponding slow-fast geometry of system Eq. (1), see also Ref. [24]. Following the classical approach (see, e.g., Ref. [18]), we find the fold condition for the two-dimensional critical manifold as

$$\left(1 - v_1^2\right)\left(1 - v_2^2\right) = c\left(2 - v_1^2 - v_2^2\right).$$

For $c = 0$, this provides two lines of folds, intersecting at the point $v_1 = v_2 = -1$. At $b = 1$, the symmetric equilibrium Eq. (5) passes through this intersection of folds (DH point in Fig. 2). At the same time, the slow flow across the folds vanishes along the whole pair of intersecting lines of folds and hence violates also the usual genericity assumption on a folded singularity. An unfolding at small $c \neq 0$ of this degenerate situation involves the interplay of two small quantities. As a first step, we will explore these mixed-mode type dynamics without invoking the singular limit where these two quantities tend to zero. Instead, we use simulations and numerical path-following techniques to describe the bifurcation scenario for finite values of ε. Comparing the results of the numerical bifurcation analysis for different values of ε will also provide some information about possible scalings between the two small quantities.

III. COMPLEX DYNAMICAL REGIMES AT THE CANARD TRANSITION

To numerically examine the different types of solutions of system Eq. (1), we have performed a parameter sweep with respect to b at fixed $c = -0.01$ and $\varepsilon = 0.1$; see Fig. 6. The scan is performed by a numerical continuation according to the following procedure: after each increment in the sweeping parameter b, we use the final state of the preceding simulation as an initial condition, then discard a transient, and sample the return times T_n between consecutive crossings of the Poincaré section $w_1 = -2/3$. The robustness of the numerical results has been verified for different simulation step sizes of the fourth-order Runge-Kutta scheme, which has been used in all of our simulations. Sweeping has been carried out in forward (increasing b, red points) and backward direction (decreasing b, black points), allowing us to detect potential coexisting

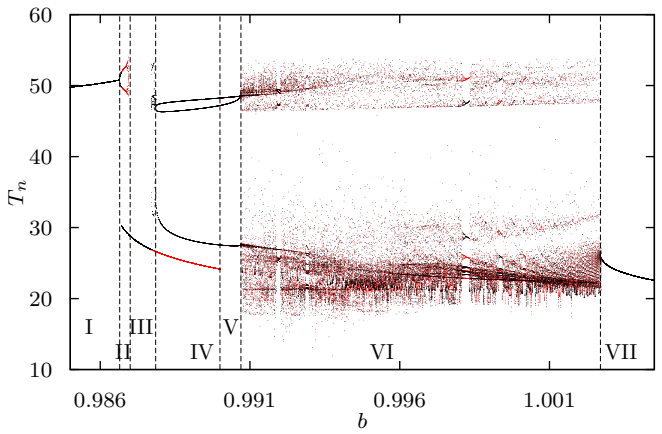

FIG. 6. Sampled return times T_n between consecutive crossings of the hyperplane $w_1 = -2/3$ for varying b and $(c, \varepsilon) = (-0.01, 0.1)$. Red and black points correspond to different sweeping directions in b.

stable regimes. Note that the return times $T_n \approx 50$ correspond to a single round trip of the unit $j = 1$ along the relaxation oscillation orbit, while the return times $T_n < 30$ correspond to a round trip following a subthreshold oscillation orbit. In Fig. 6, one can identify the regime of successive spiking in regions I and II, the in-phase subthreshold oscillations in regions II–IV, and the antiphase subthreshold oscillations in region VII. In addition, we find the periodic regime displayed in Fig. 7(a), which is the only attractor in region V and coexists with the in-phase subthreshold oscillations in region IV. Note that due to the space-time symmetry Eq. (6), the phase portraits of the trajectories of both units in the (v, w) plane coincide. This periodic regime can be characterized as follows. Within one period, each unit performs two round trips along the relaxation oscillation orbit and one round trip along a subthreshold oscillation orbit. The spikes of the two units again occur with a phase shift as in the successive spiking regime. However, as a result of the inlaid subthreshold oscillations, the spiking order gets reversed for every pair of successive relaxation oscillations. This regime of alternating spiking order with a single subthreshold oscillation performed between each pair of successive spikes is referred to as *simple leap-frogging*. We shall discuss the underlying bifurcation scenario and its dependence on the slow-fast structure of the system in the following section.

In region VI, one observes chaotic behavior, interrupted by some small parameter intervals of more complicated periodic behavior. Chaotic mixed-mode oscillations have already been numerically observed in Ref. [29] for a periodically forced slow-fast oscillator. Examples of chaotic orbits are shown in Figs. 7(e) and 7(f). More complicated periodic orbits from some of the periodic windows in region VI are provided in Figs. 7(b)–7(d). The periodic orbits in Figs. 7(b) and 7(d) carry the space-time symmetry Eq. (6), which leads to a similar exchange in the spiking order as the leap-frog orbit in Fig. 7(a). The periodic solution in Fig. 7(c) is asymmetric, displaying successive spikes with fixed spiking order similar to Fig. 4(a), but interspersed with several almost antiphase subthreshold oscillations.

A. Simple leap-frogging

The dynamical regime of leap-frogging illustrated in Fig. 7(a) is a periodic regime where successive spikes occur with an alternating spiking order. The alternation is induced

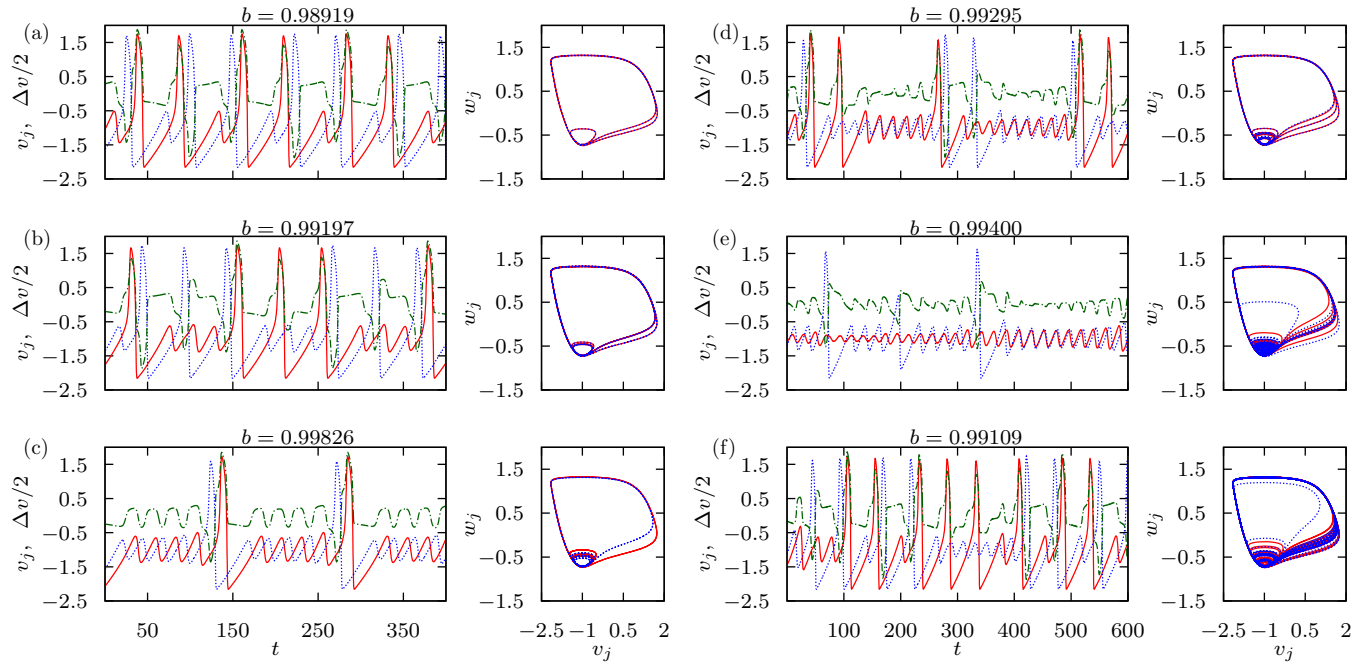

FIG. 7. Time traces and phase portraits of selected trajectories from regions V and VI in Fig. 6: Simple leap frogging in (a); periodic orbits with space-time symmetry in (b) and (d); asymmetric periodic orbit with several subthreshold oscillations in between successive spikes in (c); chaotic regimes in (e) and (f). Other parameters and colors and line styles are as described in the caption of Fig. 4.

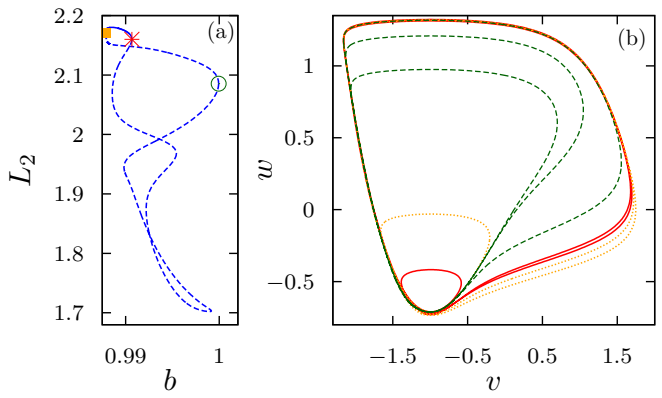

FIG. 8. (a) Branch of simple leap-frog solutions for varying b and fixed $c = -0.01$, $\varepsilon = 0.1$. The stability region (solid curve) is bounded by two folds of limit cycles (yellow square and red cross). At all other folds (e.g., green circle) both branches are unstable (dashed curves). (b) Phase portraits of limit cycles at the folds from panel (a), square (dotted), cross (solid), and circle (dashed).

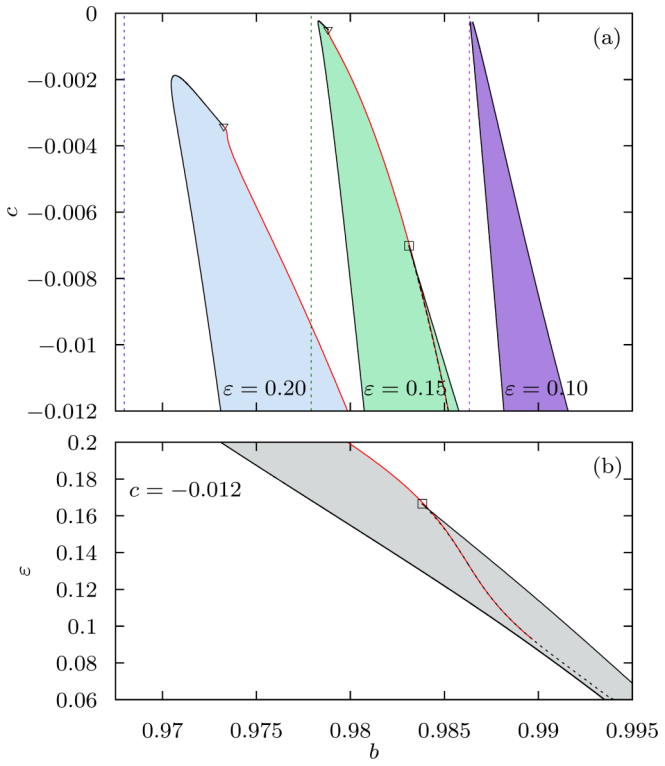

FIG. 9. (a) Stability regions of the simple leap-frog solutions in the (b, c) plane for fixed $\varepsilon \in \{0.2, 0.15, 0.1\}$ are shown in blue, green, and purple, respectively. The vertical dashed lines of corresponding color indicate the location $b_c(\varepsilon)$ of the canard transition of the synchronous oscillations. (b) Stability regions of the simple leap-frog solutions in the (b, ε) plane for fixed $c = -0.012$. In both panels, the stability regions are bounded by curves of fold bifurcations (solid black lines) and curves of pitchfork bifurcations (shown by red color). Triangles and squares indicate pitchfork-fold interaction and cusp points.

by a subthreshold oscillation of the leading unit, whereby the lagging unit, passing without such a small loop, can overtake the current leader and spike the next time first. During the next spiking event, the units follow an analogous scenario but with interchanged roles, which results in the space-time symmetry Eq. (6). Figure 8(a) provides the branch of leap-frogging solutions for varying b and fixed $(c, \varepsilon) = (-0.01, 0.1)$. The branch has the shape of a closed curve and is stable only within a small region bounded by two folds of limit cycles. A continuation of these folds in the two parameters (b, c), shown as black curves, provides the purple stability region shown in Fig. 9(a). The latter has the shape of a linear cone and points to the canard transition of the uncoupled periodic regime at $(b, c) = (b_c, 0)$. However, for the chosen value of $\varepsilon = 0.1$, the exact bifurcation structure in the vicinity of this point could not be reliably resolved numerically. Therefore, to gain a better understanding of the bifurcation structure at the tip of the stability cone, we increased the value of ε. Figure 9(b) shows the associated stability region in the (b, ε) plane. For the fixed values of $\varepsilon = 0.15$ and $\varepsilon = 0.2$, we calculated again the stability cones in the (b, c) plane, see the green and blue regions in Fig. 9(a). For these larger values of ε, it becomes apparent that the cones are clearly detached from the line $c = 0$, and that the sharp tip of the cone is actually formed by a single smooth curve of fold bifurcations. However, there is a codimension-two point close to the tip where a curve of symmetry-breaking pitchfork bifurcations crosses through the fold and becomes the stability boundary of the leap-frogging regime. The pitchfork curves are plotted in red in Fig. 9. For larger $\varepsilon = 0.15$ [see the green stability cone in Fig. 9(a)], we observe another cusp point where the branch of stable leap-frogging folds over, such that its stability region is again delineated by a fold (black curves in Fig. 9).

For $\varepsilon = 0.2$ we were able to completely resolve the bifurcation scenario in the vicinity of the tip; see Fig. 10. At small coupling $c = -0.00195$ the branch of leap-frogging solutions emerges as a small bubble [panel (I)]. For stronger coupling, this closed branch folds over and a further pair of folds emanates from a cusp point. Moreover, through symmetry-breaking pitchfork bifurcations, there appears a branch of *asymmetric* leap-frogging solutions, which is also folded in an increasingly complex fashion, sometimes even featuring a small region of stability [see panel (II)]. Another type of codimension-two bifurcation points are 1:1 resonances, which give rise to branches of torus bifurcations. Figure 9 shows that for smaller ε, this complicated bifurcation scenario is contracted to a small vicinity of the canard transition of the uncoupled periodic regime at $(b, c) = (b_c, 0)$. The presumably exponential scaling of this contraction would clarify why already for $\varepsilon = 0.1$ the bifurcations at the tip of the cone could not be reliably resolved by our numerics.

B. Multiple leap-frogging

We have observed that the stable simple leap-frog solutions emerge already at very weak negative coupling and are accompanied with a regime of complicated or chaotic mixed-mode oscillations. However, for stronger negative coupling, one finds a different scenario. In Fig. 11 we show different dynamical regimes for varying parameter b, now with $c = -0.1$, while ε is fixed again to 0.1. Similar to Fig. 6, we

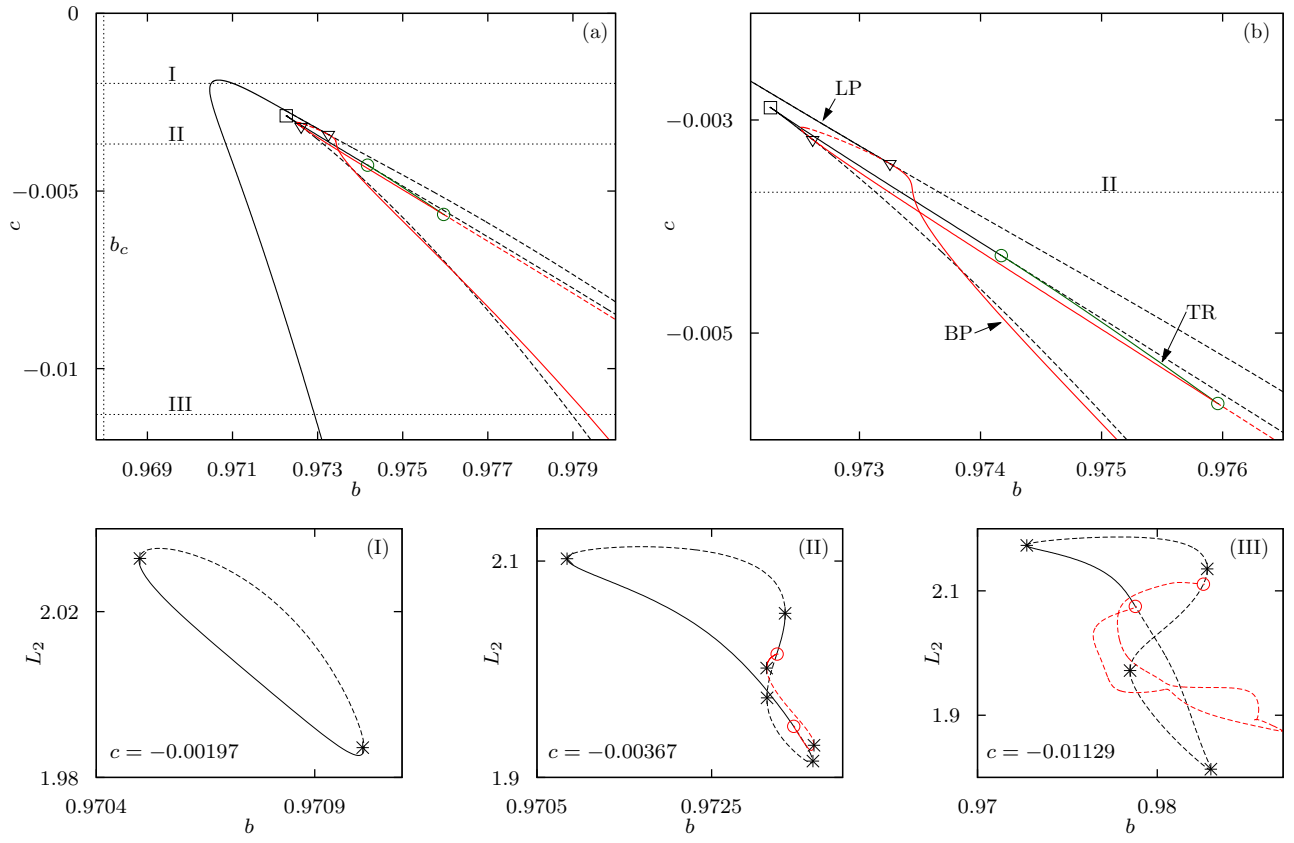

FIG. 10. (a) Bifurcations of the simple leap-frogging solutions in the (b, c) plane for $\varepsilon = 0.2$. (b) Enlarged view of the region where the complexity of the bubble increases. Bifurcation curves: folds of limit cycles (black), pitchfork bifurcations (red), torus bifurcations (green), also indicated by the labels LP, BP, and TR in panel (b), respectively. Solid curves indicate bifurcations delimiting the stability region; Dashed bifurcation curves involve only unstable states. Codimension-two bifurcations: cusps of limit cycles (squares), pitchfork-fold (triangles), torus (green circles). (I)–(III) Solid curves indicate stable branches of leap-frogging solutions with folds points (stars) and pitchfork bifurcations (circles), dashed curves indicate unstable branches. Asymmetric branches emerging from pitchfork bifurcations (red circles) are shown in red. The chosen values of c are indicated in panels (a) and (b).

have for each b value sampled the return times between consecutive Poincaré events where one of the units crosses $v_j = -b$ in increasing direction. For this stronger repulsive coupling we find a sequence of periodic patterns with a

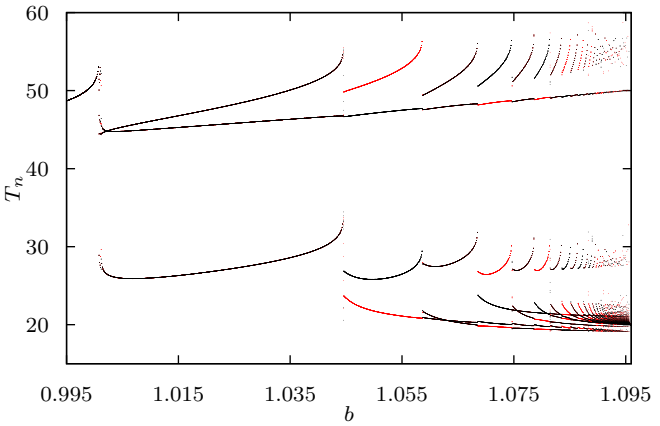

FIG. 11. Sampled return times between consecutive Poincaré events of $v_1 = -b$ (red) or $v_2 = -b$ (black) for varying b and fixed $(c, \varepsilon) = (-0.1, 0.1)$.

gradually increasing number of subthreshold oscillations between two subsequent relaxation oscillations. Beginning from the regime of successive spiking at the left edge of the diagram, the system switches to the simple leap-frogging regime, characterized by two sightly different return times $T_n \approx 50$ corresponding to round trips along the relaxation oscillation orbit and a single return time $T_n < 30$ corresponding to the subthreshold oscillation following only after every second spike. Due to the symmetry Eq. (6) and the alternating spiking order, the units leave an identical trace in the respective return times. The time traces typical for the subsequent dynamical regime at larger b are shown in Fig. 12(a). Here, the subthreshold oscillations follow after each spike, which results in an asymmetric solution with fixed leader and laggard unit, distinguished by slightly different return times for the small loop and the relaxation oscillation. Note that the subthreshold oscillations, performed almost in antiphase, allow for the units to interchange the leadership twice. This is why we call this regime *double leap-frogging*. Increasing b further, we find another regime, again with the space-time symmetry Eq. (6) and an alternating spiking order, now caused by a triple interchange of leadership while performing the small loops; see Fig. 12(b). The following periodic regimes for larger b exhibit a further increasing number of subthreshold oscillations and

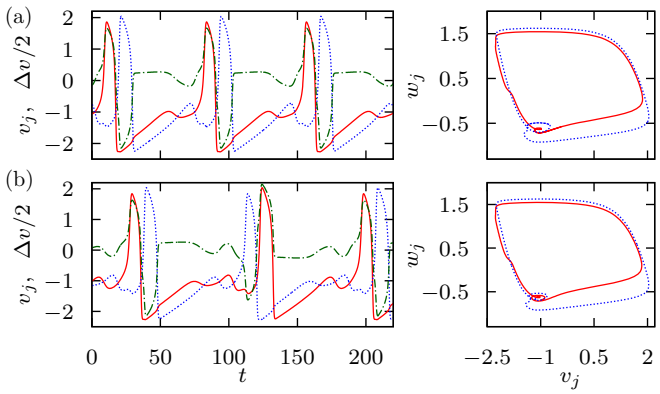

FIG. 12. Time traces and phase portraits of double leap-frogging at $b = 1.05$ (a) and triple leap-frogging at $b = 1.065$ (b). Other parameters are $(c, \varepsilon) = (-0.1, 0.1)$. Colors and line styles are as described in the caption of Fig. 4.

are successively either of the asymmetric type with fixed spiking order or of the type with the space-time symmetry and an alternating order of spiking, characterized by an even and odd number of leadership exchanges, respectively.

We have examined the stability regions of the double leap-frogging regime for varying c and different values of ε; see Fig. 13. In contrast to the case of simple leap-frogging, these regions do not extend to a close vicinity of the degeneracy at $c = 0$. Under varying ε, their position with respect to the parameter b does not adapt to the canard transition $b_c(\varepsilon)$ of the symmetric oscillations (vertical dashed lines), as in case of the simple leap-frogging. The stability boundaries are outlined

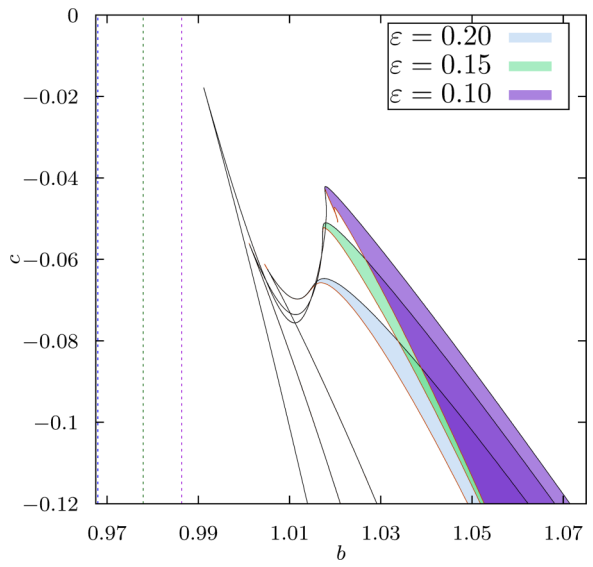

FIG. 13. Stability regions of the double leap-frog solutions in the (b, c) plane for fixed $\varepsilon \in \{0.2, 0.15, 0.1\}$ are presented in blue (bottom), green (middle), and purple (top), respectively. The left boundary of each region is given by a curve of period doubling bifurcations (orange), whereas the right one is provided by a fold curve (black). The vertical dashed lines of corresponding color indicate the location $b_c(\varepsilon)$ of the canard transition of the synchronous oscillations.

by curves of period doubling (orange) and curves of fold bifurcations (black) and do not involve any codimension-two bifurcations. This scenario for larger negative coupling, which is characterized by subsequent periodic patterns with different numbers of large relaxation oscillations and small loops, conforms, except for the different symmetry types, to the results of the asymptotic theory of mixed-mode oscillations at a folded node singularity.

IV. DISCUSSION AND OUTLOOK

In the present study, we have demonstrated that a variety of complex leap-frog patterns may emerge in a simple system comprised of two FitzHugh-Nagumo units with linear repulsive coupling in the fast variables. This complex dynamical scenario appears for parameter values in a vicinity of the canard transition of the uncoupled system and involves periodic solutions of different symmetry types. For larger repulsive coupling we obtain periodic regimes combining different numbers of small subthreshold and large relaxation oscillations, which resemble the general results for mixed-mode oscillations in slow-fast systems. For almost vanishing coupling, where the system gains an additional degeneracy, the situation is different. The stability region of the regime of simple leap frogging has the shape similar to a locking cone that approaches extremely close to the canard transition at vanishing coupling. Close to the tip of the cone, we have found a complex bifurcation scenario, which for decreasing ε is contracted to a close vicinity of the degenerate canard at $c = 0$. This contraction happens at a very fast and presumably exponential rate, such that already for moderately small values of ε a reliable numerical treatment became unfeasible and it would be a challenging task to perform an analytical study of this scenario in the singular limit $\varepsilon \to 0$.

Qualitatively, the onset of the leap-frog patterns may be explained as a result of a strong sensitivity to perturbations of the relaxation oscillation of a single FitzHugh-Nagumo unit just above the canard transition. There, already very small perturbations applied during the passage near the fold singularity of the slow manifold can deviate the trajectory away from the relaxation oscillation, giving rise to one or several loops conforming to subthreshold oscillations. Such a behavior of phase-sensitive excitability and the resulting response to excitations by noise of a single FitzHugh-Nagumo unit has been studied in Ref. [30]. Similar phenomena where the excitations arise from interactions in more complex networks have been studied in Ref. [31].

So far, the conditions relevant for the emergence of leap-frog patterns have mostly been considered within the context of neuroscience, especially in terms of relation to synchronized states. It has been known that such patterns cannot be obtained within the framework of weak-coupling theory for a pair of phase oscillators, because alternating order of firing cannot be described by reduction to an autonomous flow on the corresponding torus [32–34]. Thus, it was first believed that to observe the leap-frog solutions, one has to complement the phase oscillator dynamics by a complex synaptic coupling involving a finite synaptic time constant [12]. The suggested alternative has been to augment the simple phase dynamics by an additional negative phase branch

corresponding to strong hyperpolarization after the spiking event, as in case of the quadratic integrate-and-fire neuron model [12]. With regard to relaxation oscillators, the leap-frog patterns have first been observed as near-synchronous states where the complete phase synchronization is perturbed by *strong* inhibitory or excitatory coupling [13,14]. Later research focused on class I neural oscillators represented by Wang-Buszáki [15] or Morris-Lecar model [12,35]. In both instances, it has been found that the appropriate inhibitory noninstantaneous synaptic dynamics is crucial for the onset of leap-frog dynamics. In particular, in the case of Morris-Lecar oscillators, such patterns are facilitated by the fact that the strong coupling causes the neurons to become transiently trapped in the subthreshold (excitable) state during a certain interval of the oscillation cycle, which allows for the exchange of the spiking order between the units [12]. In contrast to the above studies, we do not suggest a specific physiological mechanism, but discuss the general case of a system of *weakly* coupled *excitable* units and show how the mechanism behind the exchange of leadership involves subthreshold oscillations, typically observed in class II neural oscillators [17,18,20]. In this sense our small negative linear coupling term can be seen as the essence of how qualitatively a local linearization of a more complicated functional dependence has to act to induce the leap-frog patterns.

ACKNOWLEDGMENTS

This work was supported by the Ministry of Education, Science, and Technological Development of Republic of Serbia under Project No. 171017, the DAAD Serbia-Germany Bilateral Project "Emergent Dynamics in Systems of Coupled Excitable Units," as well as the DFG within the framework of Collaborative Research Center SFB 910. The authors thank O. E. Omel'chenko and N. Semenova for fruitful discussions.

[1] R. C. Elson, A. I. Selverston, R. Huerta, N. F. Rulkov, M. I. Rabinovich, and H. D. I. Abarbanel, Phys. Rev. Lett. **81**, 5692 (1998).
[2] R. Milo, S. Shen-Orr, S. Itzkovitz, N. Kashtan, D. Chklovskii, and U. Alon, Science **298**, 824 (2002).
[3] E. Bullmore and O. Sporns, Nat. Rev. Neurosci. **10**, 186 (2009).
[4] O. Sporns, *Networks of the Brain* (MIT Press, Cambridge, MA, 2011).
[5] S. Song, P. J. Sjostrom, M. Reigl, S. Nelson, and D. B. Chklovskii, PLoS Biol. **3**, e68 (2005).
[6] A. Pikovsky, M. Rosenblum, and J. Kurths, *Synchronization, a Universal Concept in Nonlinear Science* (Cambridge University Press, Cambridge, UK, 2003).
[7] E. M. Izhikevich, *Dynamical Systems in Neuroscience: The Geometry of Excitability and Bursting* (MIT Press, Cambridge, MA, 2007).
[8] D. Terman, E. Lee, J. Rinzel, and T. Bem, SIAM J. Appl. Dynam. Syst. **10**, 1127 (2011).
[9] G. Buzsáki, *Rhythms of the Brain* (Oxford University Press, Oxford, 2009).
[10] P. Goel and G. B. Ermentrout, Physica D (Amsterdam) **163**, 191 (2002).
[11] C. D. Acker, N. Kopell, and J. A. White, J. Comp. Neurosci. **15**, 71 (2003).
[12] M. Oh and V. Matveev, J. Comput. Neurosci. **26**, 303 (2009).
[13] A. Bose, N. Kopell, and D. Terman, Physica D (Amsterdam) **140**, 69 (2000).
[14] Y. D. Sato and M. Shiino, Phys. Rev. E **75**, 011909 (2007).
[15] S. K. Maran and C. C. Canavier, J. Comput. Neurosci. **24**, 37 (2008).
[16] D. Terman, J. E. Rubin, and C. O. Diekman, Chaos **23**, 046110 (2013).
[17] M. Desroches, J. Guckenheimer, B. Krauskopf, C. Kuehn, H. M. Osinga, and M. Wechselberger, SIAM Rev. **54**, 211 (2012).
[18] C. Kuehn, *Multiple Time Scale Dynamics* (Springer International Publishing, Switzerland, 2015).
[19] E. N. Davison, Z. Aminzare, B. Dey, and N. E. Leonard, Chaos **29**, 033105 (2019).
[20] M. Desroches, B. Krauskopf, and H. M. Osinga, Chaos **18**, 015107 (2008).
[21] M. Krupa, B. Ambrosio, and M. A. Aziz-Alaoui, Nonlinearity **27**, 1555 (2014).
[22] E. Köksal Ersöz, M. Desroches, and M. Krupa, Physica D (Amsterdam) **349**, 46 (2017).
[23] M. N. Stolyarov, V. A. Romanov, and E. I. Volkov, Phys. Rev. E **54**, 163 (1996).
[24] J. Guckenheimer, K. Hoffman, and W. Weckesser, Int. J. Bifurcat. Chaos **10**, 2669 (2000).
[25] E. J. Doedel, and B. E. Oldeman, *AUTO-07P: Continuation and Bifurcation Software for Ordinary Differential Equations* (Concordia University, Montreal, 2012).
[26] S. M. Baer and T. Erneux, SIAM J. Appl. Math. **46**, 721 (1986).
[27] V. A. Makarov, V. I. Nekorkin, and M. G. Velarde, Phys. Rev. Lett. **86**, 3431 (2001).
[28] B. Lindner, J. Garcia-Ojalvo, A. Neiman, and L. Schimansky-Geier, Phys. Rep. **392**, 321 (2004).
[29] K. Shimizu, Y. Saito, M. Sekikawa, and N. Inaba, Physica D (Amsterdam) **241**, 1518 (2012).
[30] I. Franović, O. E. Omel'chenko, and M. Wolfrum, Chaos **28**, 071105 (2018).
[31] G. Ansmann, K. Lehnertz, and U. Feudel, Phys. Rev. X **6**, 011030 (2016).
[32] M. Golubitsky, K. Josic, and E. Shea-Brown, J. Nonlin. Sci. **16**, 201 (2006).
[33] E. M. Izhikevich, and Y. Kuramoto, Weakly coupled oscillators, Encycl. Math. Phys. **5**, 448 (2006).
[34] F. C. Hoppensteadt and E. M. Izhikevich, *Weakly Connected Neural Networks* (Springer, New York, 1997).
[35] *Frontiers of Applied and Computational Mathematics*, edited by D. Blackmore, A. Bose, and P. Petropoulos (World Scientific, Singapore, 2008).